RSC Advances

PAPER

View Article Online
View Journal | View Issue



Cite this: *RSC Adv.*, 2022, **12**, 27820

# Pure copper nanoparticles prepared by coating-assisted vapor phase synthesis without agglomeration†

Yong-Su Jo,[ab] Hye-Min Park,[a] Gwang-Hwa Jin,[ab] Bhabani Sankar Swain,*[a] Seok-Hong Min,[c] Young Keun Kim *[b] and Seung-Min Yang*[a]

Received 23rd August 2022
Accepted 9th September 2022

DOI: 10.1039/d2ra05281d

rsc.li/rsc-advances

Modern electronic devices, such as smartphones and electric vehicles, require multilayer ceramic capacitors (MLCCs), which comprise highly pure Cu terminations and Ni electrodes. Vapor-phase synthesis (VPS) is a promising method for synthesizing nanoparticles (NPs) with high purity and crystallinity. However, the agglomeration of the NPs occurs during their synthesis, which degrades the performance of the MLCC electrodes owing to several factors, including electrical shorts and low packing density. This paper proposes a coating-assisted VPS to inhibit agglomeration using potassium chloride (KCl) as the coating agent. The agglomeration ratio of the Cu NPs synthesized by in-flight coating with KCl at 950 °C significantly decreased from 48.20% to 3.80%, compared to without KCl coating. Furthermore, X-ray fluorescence and X-ray diffraction analyses confirmed that the KCl coating agent and residual copper chloride were removed by washing with ammonium hydroxide.

## 1 Introduction

Cu nanoparticles (NPs) have been of great interest in various applications, such as catalysts,[1,2] electrodes,[3,4] energy conversion, and storage.[5,6] In addition, Cu NPs are widely used as electrodes for electronic components, such as multilayer ceramic capacitors (MLCC), because of their high electrical conductivity and reserves.[7] Various methods have been used to synthesize Cu NPs, including wet chemical synthesis[8,9] and vapor phase synthesis (VPS).[10–13] According to the high integration of electronic components, Cu prepared by VPS is preferred in industrial applications over wet chemical synthesis, which can cause defects owing to the residual carbon and low crystallinity.

VPS is performed at high temperatures without the use of surfactants. Therefore, Cu NPs with high purity and crystallinity can be synthesized using VPS. However, a large number of agglomerated particles are generated by the active collision between particles, which are undesirable for MLCC electrodes because of several factors, including electrical shorts and low packing density. However, inhibiting the formation of agglomerates[14–16] is difficult in VPS because surfactants cannot be used in this method owing to the high process temperature. Therefore, Cu NPs prepared by VPS must undergo a classification process, resulting in a low yield.[17] This study focused on fabricating non-agglomerated Cu NPs using the in-flight method during chemical vapor synthesis (CVS).

In VPS, NPs are sequentially prepared by nucleation, growth, and coagulation. The agglomeration of the particles, which affect the yield, was determined during the coagulation step. The coagulation frequency increases as the reaction and feed rates of the particle increase, temperature increases, or mass of individual particles decreases. The particles are usually coagulated into spherical particles through full coalescence or into chain-like agglomerated particles through partial coalescence. Complete coalescence occurs when the particle size is less than the critical size depending on the sufficient temperature residence time and material.[14,15,18,19] Previous studies have attempted to inhibit aggregation during VPS through gas quenching.[20,21] However, gas quenching is expensive owing to high gas usage. Moreover, this method cannot rapidly and uniformly lower the temperature as the reactor size increases. Another representative method is vapor-phase coating,[22,23] which can sufficiently suppress the agglomeration of particles during flame synthesis. However, the process parameters, such as coating thickness and temperature, cannot be independently controlled because the coating agent NaCl is formed by the reaction of the reducing agent Na and precursor metal salt. In addition, Na, which is difficult to handle owing to its high reactivity, also limits the process.

[a]*Functional Materials and Components R&D Group, Korea Institute of Industrial Technology, Gangneung 25440, Gangwon-do, Republic of Korea*

[b]*Department of Materials Science and Engineering, Korea University, Seoul 02841, Republic of Korea*

[c]*Korea Institute of Industrial Technology Interdisciplinary Program, Gangneung-Wonju National University, Gangneung 25457, Gangwon-do, Republic of Korea*

† Electronic supplementary information (ESI) available. See https://doi.org/10.1039/d2ra05281d

In this study, we injected a separate coating agent to independently control the coating thickness and temperature. Moreover, we observed the effects of the amount and temperature of the coating agent on the particle agglomeration during VPS. We considered metal chlorides as the coating agent candidates for the following reasons. First, the selected coating agent must have an appropriate vapor pressure to induce condensation within the target temperature range. Second, the thermal decomposition and reaction should not occur at a reactor temperature of 1000 °C. Third, the coating agent should be easily removed by washing. To suppress particle agglomeration with this selected nonreactive coating agent, an in-flight coating method was attempted in the cooling section of 850–950 °C. Finally, we reported the synthesis of high-purity and highly crystalline Cu NPs, including post-treatment chemical washing.

## 2 Experimental

Coating-assisted CVS was used to prepare the Cu NPs. We employed a vertical hot-wall reactor for CVS at a fixed heating zone temperature of 1000 °C. CuCl (Alfa Aesar, 97%) and KCl (Sigma Aldrich, 99.0%) were simultaneously injected into the reactor using a powder feeder (Rovo, Fine Techniques) with a $N_2$ carrier gas flow rate of 3.21 standard liter per minute (SLM).

Table 1 shows the variations in the coating temperature with the coating agent content and feed rate. As the coating temperature is the starting temperature of the condensation of the evaporated coating agent, the content of the coating agent was determined using the saturated vapor pressure at the coating temperature. The CuCl feed rate was kept constant at 36.4 g $h^{-1}$. The KCl feed rate was varied. The reducing gas $H_2$ was injected directly into the particle formation section at a flow rate of 1 SLM. We reduced the temperature by quenching $N_2$ gas in the cooling section. CuCl and KCl evaporated in the evaporation section. CuCl vapor was mixed with $H_2$ in the particle formation section, and underwent reduction, nucleation, growth, and coagulation to form Cu NPs. The coagulated NPs completely coalesced in the particle formation section. Partial coalescence occurred primarily in the cooling section. We recovered the Cu NPs produced by the CVS in a powder collector (Bag filter) outside the reactor. A schematic of the CVS reactor used in our experiment is presented in the ESI (Fig. S1).† Prepared Cu NPs samples were sonicated in $NH_4OH$ using ultrasonicator (Q500, Qsonica) to remove residual CuCl and KCl. After washing, the NPs were obtained by centrifugal separation at 8000 rpm. The microstructure of the Cu NPs was analyzed using field-emission scanning electron microscopy (FESEM, Quanta 250 FEG, FEI). Au–Pd thin films were sputtered on the Cu NPs to obtain high-quality FESEM images. We performed image analysis using FESEM images of the dispersed particles as a monolayer on a substrate. The geometric standard deviation (GSD) and count median diameter (CMD) of the Cu NPs were determined by the image analysis of 200 particles. The agglomeration ratio was calculated by dividing the number of primary particles, constituting the agglomerate, by the sum of primary particles constituting the agglomerate and non-agglomerating particles, which were obtained through the image analysis of more than 500 particles. The details of the calculation method are provided in eqn (1)–(3) in the ESI.† The surface chemical composition of Cu NPs coated with KCl at 950 °C was examined by energy-dispersive X-ray spectroscopy (EDS) elemental mapping. We characterized the phases of the Cu NPs by X-ray diffraction (XRD, Empyrean, Panalytical). The chemical compositions of the as-prepared and post-washed Cu NPs were examined using X-ray fluorescence (XRF, M4 TORNADO, Bruker).

## 3 Results and discussion

In this study, an in-flight coating method in a cooling section at 850–950 °C was developed in an attempt to suppress particle agglomeration. We calculated the Gibbs free energy change for the hydrogen reduction reaction of several metal chlorides, namely CuCl(g), $ZnCl_2$(g), KCl(g), LiCl(g), $MgCl_2$(g), NaCl(g), $CaCl_2$(g), and $NiCl_2$(g), using Thermo-Calc DB.[24]

Fig. 1 shows the Gibbs free energy changes with the temperature (500–1000 °C) of the hydrogen reduction for various metal chloride reactions. The Gibbs free energy changes with temperature of $ZnCl_2$(g), KCl(g), LiCl(g), $MgCl_2$(g), NaCl(g), $CaCl_2$(g), and $NiCl_2$(g) were reproduced from our previous report[24] and CuCl (present study) are presented. If a particular metal chloride does not react with $H_2$, it will not react with Cu. The negative Gibbs free energy change of CuCl(g) indicates that CuCl(g) is expected to react with $H_2$.

Fig. 2 shows the saturated vapor pressures of CuCl(g), $ZnCl_2$(g), KCl(g), LiCl(g), $MgCl_2$(g), NaCl(g), $NiCl_2$(g), and $CaCl_2$(g) with temperature, calculated using the Antoine coefficients,[25] as previously discussed.[24] A coating agent with high vapor pressure inhibits the agglomeration of the NPs by increasing the distance between the Cu cores. However, an excessively high vapor pressure of the coating agent lowers the

Table 1 Synthesis conditions for saturated vapor pressure control of coating agents

| Sample number | Feed rate of feedstock (g $h^{-1}$) | Content of coating agent in feedstock (wt%) | Vapor pressure of coating agent (kPa) | Coating temperature (°C) |
|---|---|---|---|---|
| | | KCl | KCl | |
| 1 | 36.40 | — | — | — |
| 2 | 37.89 | 0.05 | 0.23 | 850 |
| 3 | 43.78 | 0.26 | 1.14 | 950 |

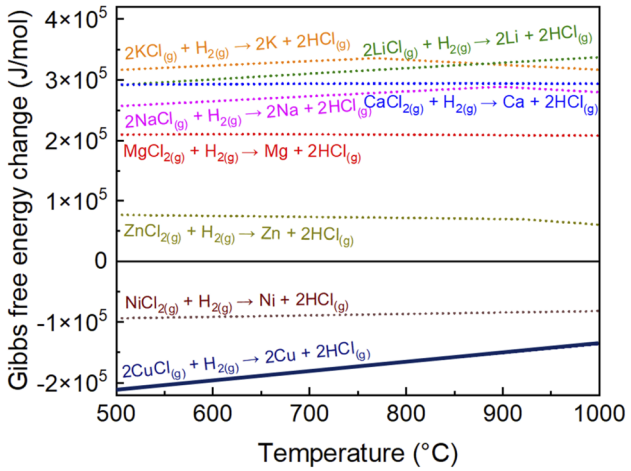


Fig. 1 Gibbs free energy changes with the temperature (500–1000 °C) of hydrogen reductions.

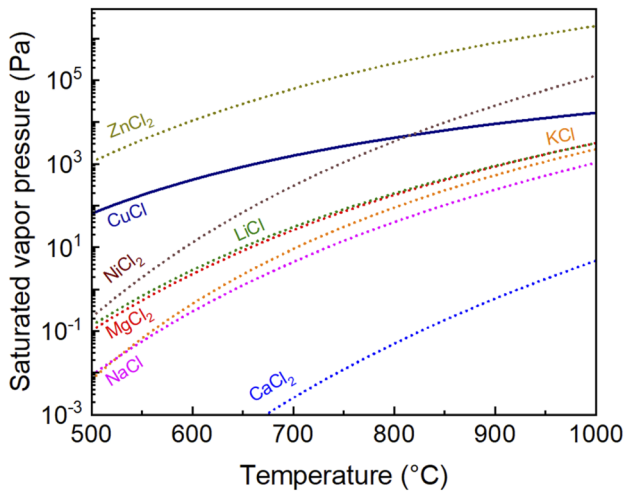


Fig. 2 Saturated vapor pressures of metal chlorides at various temperatures.

partial pressure of CuCl, which may inhibit the Cu NP reduction reaction.

Table 1 presents the processing parameters of the pure and KCl-coated Cu NPs. Fig. 3(a) and (b) show the FESEM images and particle distributions of the uncoated pure Cu NPs (Sample 1) prepared by conventional VPS, respectively. For pure Cu NPs, the GSD was 1.24, and the CMD was 205 nm. The agglomeration ratio of this sample was 48.20%, and 62, 25, 8, and 2 agglomerates had two, three, four, and five primary particles, respectively.

Fig. 3(c) and (d) show the microstructure and particle size distribution of the Cu NPs coated with KCl at 850 °C (Sample 2). At the coating temperature of 850 °C, the KCl-coated Cu NPs had a GSD of 1.24 and CMD of 254 nm. The agglomeration ratio was 10.40%. The number of agglomerates consisting of two, three, four, and five primary particles was 18, 4, 1, and 0, respectively. Similarly, Fig. 3(e) and (f) show the microstructure

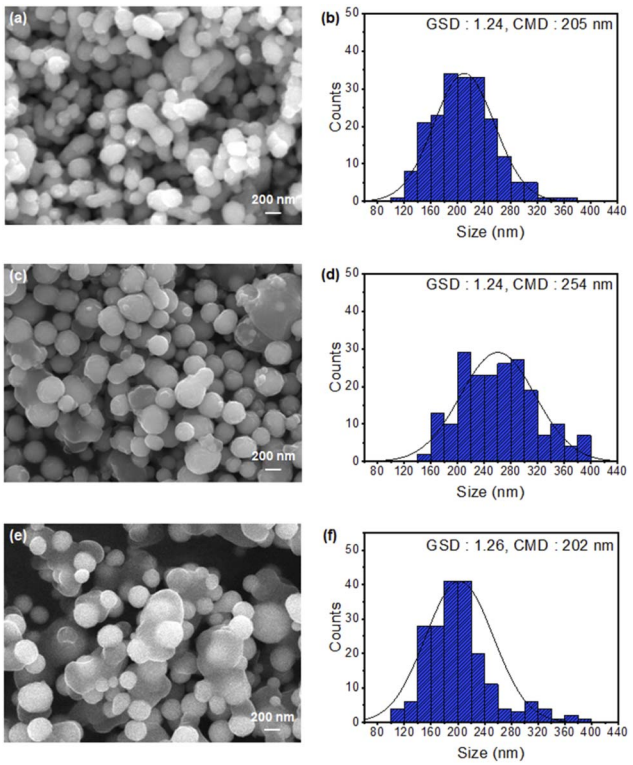


Fig. 3 FESEM images and size distribution histograms of the KCl-coated Cu NPs at different coating temperatures; (a, b) pure (sample 1), (c, d) 850 °C (sample 2), and (e, f) 950 °C (sample 3). CMD: count median diameter, GSD: geometric standard deviation, respectively.

and particle size distribution of the Cu NPs coated with KCl at 950 °C (Sample 3). At the coating temperature of 950 °C, the KCl-coated Cu NPs had a GSD of 1.26 and CMD of 202 nm. The agglomeration ratio was 3.80%. The number of agglomerates consisting of two, three, four, and five primary particles was 8, 1, 0, and 0, respectively. As the coating temperature was increased from 850 to 950 °C, the agglomeration ratio decreased from 10.40% to 3.80%. Thus, the agglomeration of the Cu NPs could be effectively inhibited by coating them with KCl. The high saturated vapor pressure of KCl sufficiently suppressed agglomeration by forming a relatively thick KCl coating on core Cu NPs,[24] which is discussed in a later section.

The agglomeration ratios, CMD, and GSD of samples 1–3 are summarized in Table 2. Fig. 4 shows the EDS elemental mapping of the Cu NPs coated with KCl at 950 °C. The identified elements were 9.16 wt% Cl, 7.82 wt% K, and 83.02 wt% Cu.

Table 2 Count median diameters (CMDs), geometric standard deviations (GSDs), and agglomeration ratios of samples

| Sample number | CMD (nm) | GSD | Agglomeration ratio (%) |
|---|---|---|---|
| 1 | 205 | 1.24 | 48.20 |
| 2 | 254 | 1.24 | 10.40 |
| 3 | 202 | 1.26 | 3.80 |

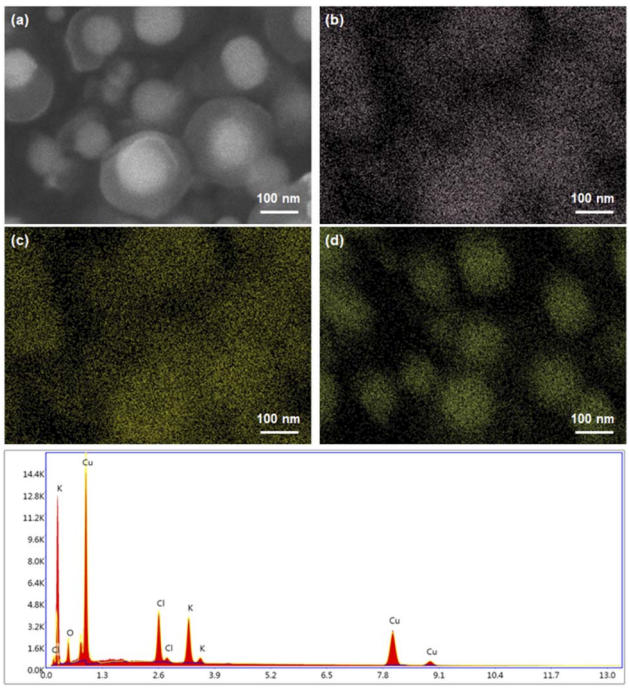


Fig. 4 EDS elemental mapping of the KCl-coated Cu NPs, including the (a) FESEM images: (b) Cl, (c) K, and (d) Cu.

From the FESEM images in Fig. 4(a), the KCl coating layer surrounding the Cu core was separated, which can be explained by the large penetration depth at a high accelerating voltage with a low atomic number.[26]

XRD analysis was performed to ensure the quality of the Cu NPs synthesized by CVS under different processing conditions. Fig. 5 shows the XRD patterns of the Cu NPs synthesized under different conditions, as shown in Table 1. We matched the XRD peak positions of our results with the JCPDS data for Cu (JCPDS 04-0836), CuCl (JCPDS 77-2383), and KCl (JCPDS 41-1476). The peaks at 43.3°, 50.5°, and 74.2° correspond to the (111), (002), and (022) planes of Cu, respectively. Residual CuCl and KCl were observed in the prepared KCl-coated Cu NPs. The peaks at 28.5°, 47.4°, and 56.3° represent the (111), (022), and (113) planes of CuCl, respectively. A small amount of KCl was observed in the KCl-coated Cu NPs. The peaks at 40.6° and 66.43° represent the (200) and (420) planes of KCl, respectively.

Appropriate chemicals should remove CuCl and KCl from the outer shell of the Cu NPs to ensure their purity. Ammonium hydroxide ($NH_4OH$) is a better candidate for removing the residual chlorine content than deionized water, which causes the oxidation of Cu NPs.[27] The prepared Cu NPs were sonicated in $NH_4OH$ using an ultra-sonicator to remove residual CuCl and KCl. The role of ammonium hydroxide and its mechanism are given in the ESI.† After washing, the NPs were obtained by centrifugal separation at 8000 rpm and characterized by XRF.

Fig. 6(a) shows the XRD patterns of the KCl-coated Cu NPs with the coating temperatures of 950 °C and after $NH_4OH$ washing. The XRD peaks of KCl and CuCl were found in the KCl-coated Cu NPs at a coating temperature of 950 °C but not in the Cu NPs after $NH_4OH$ washing. Fig. 6(b) shows the XRF results of the Cu NPs before and after $NH_4OH$ washing. Table 3 presents the compositions of the individual elements (Cu, Cl, and K) of Cu NPs synthesized by CVS before and after $NH_4OH$ washing. Only Cu and Cl were observed in the pure Cu NPs. However, Cu, Cl, and K were observed in the KCl-coated Cu NPs at 850 and 950 °C. Cu contents of 99.97 and 99.94 wt%, and Cl contents of 0 and 0 wt% were obtained in samples 2 and 3, respectively, after washing. Therefore, the KCl content used for coating could be removed by $NH_4OH$.

We further analyzed the microstructure and particle size distribution of the Cu NPs coated with KCl at 950 °C after $NH_4OH$ washing (Fig. 7). The GSD and CMD values were 1.19 and 247 nm, respectively. The number of agglomerates consisting of two, three, four, and five primary particles was 8, 1, 0, and 0, respectively. The agglomeration ratio was 3.80%.

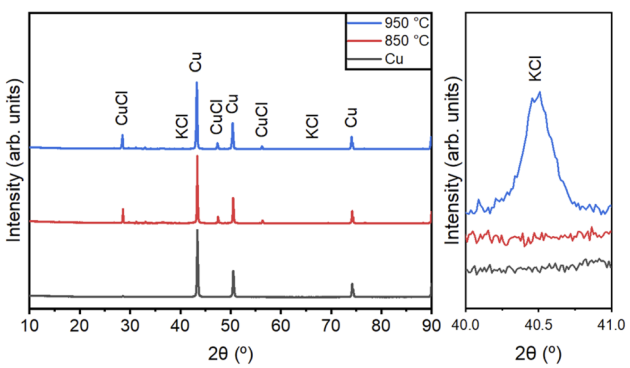


Fig. 5 XRD patterns of the pure and KCl-coated Cu NPs with coating temperatures of 850 and 950 °C.

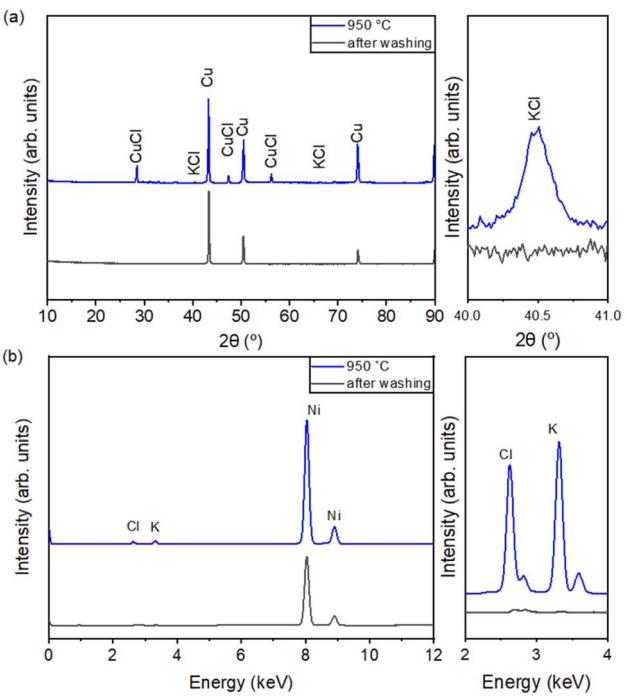


Fig. 6 (a) XRD and (b) XRF of the KCl-coated Cu NPs with the coating temperatures of 950 °C and after $NH_4OH$ washing.

Table 3 Chemical composition (wt%) of Cu-NPs of as-prepared and after $NH_4OH$ washing

| | Chemical composition (wt%) | | | | | |
|---|---|---|---|---|---|---|
| | As-prepared | | | After-washing | | |
| Sample number | Cu | K | Cl | Cu | K | Cl |
| 1 | 98.75 | — | 1.25 | 100 | — | — |
| 2 | 94.22 | 1.76 | 4.02 | 99.97 | 0.03 | — |
| 3 | 83.99 | 7.43 | 8.58 | 99.94 | 0.06 | — |

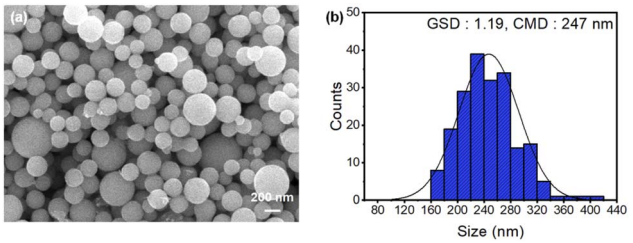


Fig. 7 (a) FESEM image and (b) particle size distribution histogram of the KCl-coated Cu NPs after $NH_4OH$ washing.

## 4 Conclusions

We synthesized Cu NPs by in-flight coating-assisted CVS using KCl as the agglomeration inhibitor. Compared to conventional CVS with an agglomeration ratio of 48.20%, the KCl inhibitor reduced the agglomeration ratio to 3.80% at 950 °C. Furthermore, the KCl inhibitor used in this study was removed by $NH_4OH$ washing, thereby achieving pure Cu NPs. Thus, we confirmed that coating-assisted CVS can inhibit the formation of agglomerates during synthesis of Cu NPs. We also believe that this method can be used for the vapor-phase synthesis of various particles.

## Author contributions

Yong-Su Jo: conceptualization, methodology, validation, investigation, formal analysis, data curation, visualization, writing-original draft preparation. Hye-Min Park: validation, investigation, data curation. Gwang-Hwa Jin: validation, investigation, data curation. Bhabani Sankar Swain: formal analysis, writing-review and editing. Seok-Hong Min: supervision, writing-review and editing. Young Keun Kim: supervision, writing-review and editing. Seung-Min Yang: conceptualization, methodology, resources, supervision, project administration, funding acquisition, writing-review and editing.

## Conflicts of interest

There are no conflicts to declare.

## Acknowledgements

This study was supported by the Korea Evaluation Institute of Industrial Technology (KEIT, grant no. 20011040), the Korea Institute of Industrial Technology (KITECH, grant no. UR-22-0003) and the Ministry of Trade, Industry and Energy (MOTIE) of the Republic of Korea.

## Notes and references

1 M. B. Gawande, A. Goswami, F. X. Felpin, T. Asefa, X. Huang, R. Silva, X. Zou, R. Zboril and R. S. Varma, Cu and Cu-based nanoparticles: synthesis and applications in catalysis, *ACS Chem. Rev.*, 2016, **116**, 3722–3811.

2 S. Munir and A. Gul, An overview of strategic non-biological approaches for the synthesis of cupper nanoparticles, *Acta Chemica Malaysia*, 2021, **5**, 24–37.

3 D. S. Jung, H. Y. Koo and S. E. Wang, Ultrasonic spray pyrolysis for air-stable copper particles and their conductive films, *Acta Mater.*, 2021, **206**, 116569.

4 S. Wu and X. Ding, Preparation of fine copper powder with chemical reduction method and its application in MLCC, *IEEE Trans. Adv. Packag.*, 2007, **30**, 1521–3323.

5 A. Khan, A. Rashid, R. Younas and R. Chong, A chemical reduction approach to the synthesis of copper nanoparticles, *Int. Nano Lett.*, 2016, **6**, 21–26.

6 B. Devadas, A. P. Periasamy and K. Bouzek, A review on poly(amidoamine) dendrimer encapsulated nanoparticles synthesis and usage in energy conversion and storage application, *Coord. Chem. Rev.*, 2021, **444**, 214062.

7 K. Hong, T. H. Lee, J. M. Suh, S. -H. Yoon and H. W. Jang, Perspectives and challenges in multilayer ceramic capacitors for next generation electronics, *J. Mater. Chem. C*, 2019, **7**, 9782–9802.

8 N. Nagar and V. Devra, Green synthesis and characterization of copper nanoparticles using Azadirachta indica leaves, *Mater. Chem. Phys.*, 2018, **213**, 44–51.

9 S. A. Patil, C. Ryu and H. Kim, Synthesis and characterization of copper nanoparticles (Cu-NPs) using rongalite as reducing agent and photonic sintering of Cu-Nps ink for printed electronics, *Int. J. Precis. Eng.*, 2018, **5**, 239–245.

10 P. G. Jamkhande, N. W. Ghule, A. H. Bamer and M. G. Kalaskar, Metal nanoparticles synthesis: an overview on methods of preparation, advantages and disadvantages, and applications, *J. Drug Delivery Sci. Technol.*, 2019, **53**, 101174.

11 N. Kulbe, O. Hofft, A. Ulbrich, S. Z. E. Abedin, S. Krischok, J. Janek, M. Polleth and F. Endres, Plasma electrochemistry in 1-butyl-3-methylimidazolium dicyanamide: copper nanoparticles from CuCl and $CuCl_2$, *Plasma Processes Polym.*, 2011, **8**, 32–37.

12 R. E. Zhumadylov, A. T. Zhunisbekov, T. S. Ramazanov, S. A. Orazbayev and M. T. Gabdullin, Obtaining of copper nanoparticles in combined RF + DC discharge plasma, *Int. J. Nanotechnol.*, 2019, **16**, 1–3.

13 P. V. Krasovskii, A. V. Samokhin, A. A. Fadeev and N. V. Alexeev, Thermal evolution study of nonmetallic impurities and surface passivation of Cu nanopowders produced via a DC thermal plasma synthesis, *Adv. Powder Technol.*, 2016, **27**, 1669–1676.

14 N. K. Roy, C. S. Foong and M. A. Cullinan, Effect of size, morphology, and synthesis method on the thermal and sintering properties of copper nanoparticles for use in microscale additive manufacturing processes, *Addit. Manuf.*, 2018, **21**, 17–29.
15 J. Feng, L. Huang, L. Ludvigsson, M. E. Messing, A. Maisser, G. Biskos and A. Schmidt-Ott, General approach to the evolution of singlet nanoparticles from a rapidly quenched point source, *J. Phys. Chem. C*, 2016, **120**(1), 621–630.
16 M. Malekzadeh and M. T. Swihart, Vapor-phase production of nanomaterials, *Chem. Soc. Rev.*, 2021, **50**, 7132–7249.
17 L. Bai, F. Yuan and Q. Tang, Synthesis of nickel nanoparticles with uniform size via a modified hydrazine reduction route, *Mater. Lett.*, 2008, **62**(15), 2267–2270.
18 K. E. Lehtinen and M. R. Zachariah, Energy accumulation in nanoparticle collision and coalescence processes, *J. Aerosol Sci.*, 2002, **33**(2), 357–368.
19 R. N. Grass, S. Tsantilis and S. E. Pratsinis, Design of high-temperature, gas-phase synthesis of hard or soft $TiO_2$ agglomerates, *AIChE J.*, 2006, **52**(4), 1318–1325.
20 S. Bianconi, M. Boselli, M. Gherardi and V. Colombo, Design-oriented modelling of different quenching solutions in induction plasma synthesis of copper nanoparticles, *Plasma Chem. Plasma Process.*, 2017, **37**, 717–738.
21 N. Y. M. Gonzalez, M. El Morsle and P. Proulx, Production of nanoparticles in thermal plasmas: a model including evaporation, nucleation, condensation, and fractal aggregation, *J. Therm. Spray Technol.*, 2008, **17**, 533–550.
22 L. Zhang, M. B. Rande and J. W. Gentry, Formation of organic coating on ultrafine silver particles using a gas-phase process, *J. Aerosol Sci.*, 2004, **35**, 457–471.
23 D. Sundaram, V. Yang and R. A. Yetter, Metal-based nanoenergetic materials: synthesis, properties, and applications, *Prog. Energy Combust. Sci.*, 2017, **61**, 293–365.
24 Y.-S. Jo, H.-J. Lee, H.-M. Park, T.-W. Na, J.-S. Jung, S.-H. Min, Y. K. Kim and S.-M. Yang, Chemical vapor synthesis of nonagglomerated nickel nanoparticles by In-Flight coating, *ACS Omega*, 2021, **6**(42), 27842–27850.
25 C. Yaws, *The Yaws Handbook of Vapor Pressure: Antoine Coefficients*, Gulf Professional Publishing, 2015.
26 L. Zarraoa, M. U. Gonzalez and A. S. Paulo, Imaging low-dimensional nanostructures by very low voltage scanning electron microscopy: ultra-shallow topography and depth-tunable material contrast, *Sci. Rep.*, 2019, **9**, 16263.
27 A. R. Martin, M. Baeyens and W. Hub, Alkaline cleaning of silicon wafers: additives for the prevention of metal contamination, *Microelectron. Eng.*, 1999, **45**, 197–208.